Title

Dark matter inelastic up-scattering with the interstellar plasma: A new source of x-ray lines, including at 3.5 keV

Journal

Physical Review D, 93(10)

ISSN

2470-0010

Authors

D'Eramo, Francesco
Hambleton, Kevin
Profumo, Stefano
et al.

Publication Date

2016-05-15

DOI

10.1103/physrevd.93.103011

Peer reviewed

Dark Matter Inelastic Up-Scattering with the Interstellar Plasma: An Exciting New Source of X-Ray Lines, including at 3.5 keV

Francesco D'Eramo,[1,2,*] Kevin Hambleton,[1,†] Stefano Profumo,[1,2,‡] and Tim Stefaniak[1,2,§]

[1] *Department of Physics, University of California, 1156 High St., Santa Cruz, CA 95064, USA*
[2] *Santa Cruz Institute for Particle Physics, Santa Cruz, CA 95064, USA*

(Dated: March 17, 2016)

We explore the phenomenology of a class of models where the dark matter particle can inelastically up-scatter to a heavier excited state via off-diagonal dipolar interactions with the interstellar plasma (gas or free electrons). The heavier particle then rapidly decays back to the dark matter particle plus a quasi-monochromatic photon. For the process to occur at appreciable rates, the mass splitting between the heavier state and the dark matter must be comparable to, or smaller than, the kinetic energy of particles in the plasma. As a result, the predicted photon line falls in the soft X-ray range, or, potentially, at arbitrarily lower energies. We explore experimental constraints from cosmology and particle physics, and present accurate calculations of the dark matter thermal relic density and of the flux of monochromatic X-rays from thermal plasma excitation. We find that the model provides a natural explanation for the observed 3.5 keV line from clusters of galaxies and from the Galactic center, and is consistent with null detections of the line from dwarf galaxies. The unique line shape, which will be resolved by future observations with the Hitomi (formerly Astro-H) satellite, and the predicted unique morphology and target-temperature dependence will enable easy discrimination of this class of models versus other scenarios for the generation of the 3.5 keV line or of any other unidentified line across the electromagnetic spectrum.

I. INTRODUCTION

The particle nature of dark matter remains a mystery. Astronomical observations can be directly used to constrain or detect certain models of particle dark matter [1]. Dark matter pair-annihilation or decay generically produces photons, either promptly or through the decay of products of the annihilation or decay event; photons also arise from the secondary emission of the produced electrons and positrons [2]. Other mechanisms producing electromagnetic emission from dark matter include, for instance, the Primakoff-like conversion of axion-like particles into photons in the presence of an external magnetic field [3].

Here, we present a completely novel mechanism to detect dark matter with astronomical observations. Our idea is that the dark matter sector consists of two physical states: a light state which is stable and is the dark matter particle, and a second, heavier state. The two dark-sector particles interact with themselves and with Standard Model particles through an effective operator which is an inelastic electric or magnetic dipole interaction term. This operator is responsible for two key features of our model:

1. the dark matter relic density, which is set almost entirely by co-annihilation processes;

2. the production of quasi-monochromatic photons, with typical energies corresponding to the mass splitting between the heavier state and the dark matter particle.

The latter process produces a detectable flux of photons if the excitation rate for the heavy particle is large, and if the heavy particle decays quickly to the dark matter particle and a photon.

In this study we explore in detail the phenomenology and properties of this *novel indirect dark matter detection channel*. In particular, we show that the thermal relic density of the dark matter is easily accommodated for the same choice of parameters for which our model predicts a detectable flux of X-ray photons from excitations of the dark matter by collisions with the interstellar plasma, and for a broad range of masses.

The signal strength predicted in our model depends on a peculiar combination of the dark matter number density times the interstellar plasma number density, which falls in the class of signal morphology explored for example in Ref. [4]. The signal also depends on the kinetic energy of the plasma particles, and thus if the plasma is in thermal equilibrium, the plasma temperature is a key factor as to whether or not the excitation rate is significant. As a result, systems such as clusters of galaxies, which host abundant dark matter and thermal plasma with characteristic temperatures of a few keV, are expected to produce bright dark matter de-excitation lines. Also, we expect to detect this line in the Milky Way center, a relatively nearby location which again possesses both large plasma and dark matter densities. However, in our scenario no signal is to be expected from local dwarf galaxies, which have very small, if any, interstellar gas. Likewise, we do not expect any signal from small, distant galaxies.

Interestingly, the generic features expected in our

*Electronic address: fderamo@ucsc.edu
†Electronic address: khamblet@ucsc.edu
‡Electronic address: profumo@ucsc.edu
§Electronic address: tistefan@ucsc.edu

model match observations of a recently discovered X-ray line at 3.5 keV, whose origin remains somewhat controversial. The line has been discovered in 2014 in observations of individual and stacked clusters of galaxies [5]. A line at the same energy was subsequently discovered in the center of the Milky Way [6], while its detection in M31 is debated and, at best, inconclusive [6–8]. On the other hand, no signal was detected neither in observations of dwarf spheroidal galaxies [9], which most notably includes recent, deep (~ 1.6 Msec) XMM observations of the Draco dwarf galaxy [10], nor in stacked observations of galaxies and groups of galaxies [11].

Some excitement arose from the detection of the 3.5 keV line based on the statement in Ref. [5] that the most plausible elemental line around 3.5 keV, from atomic de-excitation transitions of He-like potassium ions (K XVIII), would require an overabundance of K compared to solar of about 30, and thus would be "physically difficult to understand". Additionally, the energy and brightness of the line was found to be in principle compatible with what expected from the radiative decay of 7.1 keV sterile neutrinos with lifetimes of the order of 10^{29} s [5]. Other models have since then been extensively discussed in connection with a possible exotic origin of the line (see e.g. the recent review [12]).

There are convincing reasons to believe that the line does in fact originate from K XVIII transitions. The original argument in Bulbul et al [5] that this is unlikely because the required K overabundance compared to solar would be on the order of 30 is very likely incorrect for at least two reasons:

1. The K solar abundance utilized in Ref. [5] is the *photospheric* abundance, rather than the *coronal* abundance, which is about one order of magnitude larger [13] and which is the relevant quantity as a proxy to the K abundance in the interstellar medium;

2. The temperature models utilized in Ref. [5] are skewed towards large temperatures (compared for example to what inferred from same-element ratios such as Ca XIX to Ca XX) resulting in a brightness for the K line suppressed by up to one order of magnitude (see e.g. fig. 4 in Ref. [8]).

Perhaps even more critically, Ref. [14] showed that the morphology of the 3.5 keV photons from Perseus and from the Milky Way matches closely the morphology of other elemental lines, rather than what expected from, for example, dark matter decay. This morphology by itself rules out a dark matter decay interpretation for the line [14]. If an exotic origin is invoked, *the associated line emission should correlate spatially quite closely with the hot plasma in clusters and, possibly, in the Galaxy.* One such possibility is axion-like conversion in magnetic fields [15], although this scenario is not necessarily directly connected with dark matter, and the model parameters are tuned *ad hoc* to explain the observed signal.

Within the context of the scenario we consider here, it is instead natural to have a *thermal relic* dark matter candidate that produces a 3.5 keV line with (i) the required morphology, (ii) the required intensity to explain observations in clusters and in the Milky Way center, and that (iii) has suppressed emission from systems with low plasma temperatures and densities, such as dwarf galaxies.

Our model is rather economical from the standpoint of input parameters. In fact, the model is entirely defined by (1) the masses of the two particles (or, equivalently, the dark matter particle mass and the mass splitting of the heavier state), (2) the effective electric and magnetic dipole moment couplings, $c_{E,M}/\Lambda$. As we will show below, the *magnetic* dipole controls the thermal relic density (the electric dipole featuring a p-wave suppression in the co-annihilation cross section), while the *electric* dipole dominates the scattering off of free electrons and protons in the interstellar plasma (the electrons dominating the rate at low dark matter masses, $m_X \gtrsim 50$ MeV, and the protons for larger dark matter masses, $m_X \gtrsim 50$ MeV).

The scenario we discuss here generically produces a bright, detectable X-ray (or lower energy) line, with the line width given by a geometric average of the dark matter and interstellar plasma velocity dispersions. Thus, as long as the line is resolved, for example with the expected energy resolution of the recently launched Hitomi (formerly known as Astro-H) satellite [16], this scenario is observationally distinguishable and unique from both thermal plasma emission and from other new physics models.

In connection with the question of the nature of the 3.5 keV line, our models explains the observational features of the line as a result of excitations generated by the scattering of the dark matter off of electrons and protons in the thermal plasma, as long as the plasma temperature is large enough to allow the excitation transition. The resulting morphology traces the product of the plasma density and the dark matter density, in qualitative agreement with what was observed in Ref. [14]. Additionally, the dark matter particle is naturally produced as a cold thermal relic from the early universe, dominantly from coannihilation processes. Crucially, we stress that the model we propose as a possible counterpart to the 3.5 keV line can be falsified with forthcoming observations with Hitomi, and would be strikingly different than for example axion-like particle conversion or dark matter decay.

We present the results of our study as follows. We introduce in Section II the effective field theory (EFT) framework to investigate X-ray production from dark matter excitations. Such an EFT captures a large class of plausible UV completions, which we mention in what follows, and it allows a simple analysis in terms of two masses and of two coupling parameters. We identify the allowed range for these parameters in Section III, where we impose current experimental bounds. Dark matter

production in the early universe through thermal freeze-out is discussed in Section IV. With experimental and relic density constraints at hand, we finally compute the flux of X-rays from dark matter excitations and decays. General fluxes for arbitrary dark matter mass and mass splitting are presented in Section V, which ends with an analysis of the specific case of the 3.5 keV X-ray line. Conclusions are given in Section VI.

II. EFFECTIVE INTERACTIONS FOR INELASTIC DARK MATTER

We introduce a simple EFT for the dark sector of this theory. We augment the Standard Model (SM) of particles physics with two additional gauge-singlet Weyl fermions ξ and η, which are the only particles taken odd under a $\mathbb{Z}_2$ symmetry. As a consequence of this discrete symmetry, the particle corresponding to the lighter mass eigenstate is stable. The most general mass Lagrangian for the new degrees of freedom reads

$$\mathcal{L}_{\rm mass} = -\mu\,\xi\eta - \frac{1}{2}\delta_\xi\,\xi\xi - \frac{1}{2}\delta_\eta\,\eta\eta + \text{h.c.}\,. \tag{1}$$

The EFT is valid only below a cutoff scale Λ, which is interpreted as the mass of some heavy particles we integrate out to generate the effective interactions between the SM and the new fermions. The mass parameters $(\mu, \delta_\xi, \delta_\eta)$ are consistently taken below the EFT cutoff.

SM gauge invariance and the $\mathbb{Z}_2$ symmetry[1] forbid any renormalizable interaction with SM fields. The lowest-order non-renormalizable interactions one can write down are the electric and magnetic dipole moments

$$\begin{aligned}\mathcal{L}_{\rm EFT} = &-\frac{c_M}{2\Lambda}\,\overline{\psi_D}\Sigma^{\mu\nu}\psi_D\,F_{\mu\nu} + \\ &-\frac{c_E}{2\Lambda}\,\overline{\psi_D}\Sigma^{\mu\nu}\,i\gamma^5\psi_D\,F_{\mu\nu}\,.\end{aligned} \tag{2}$$

Here, we gather the two Weyl fermions ξ and η together to form a Dirac fermion ψ_D as follows:

$$\psi_D = \begin{pmatrix} \xi \\ \eta^\dagger \end{pmatrix}\,. \tag{3}$$

We also define the antisymmetric tensor

$$\frac{1}{2}\Sigma^{\mu\nu} = \frac{i}{4}\left[\gamma^\mu, \gamma^\nu\right]\,. \tag{4}$$

The operator with coefficient c_M (c_E) is a CP-even(-odd) magnetic (electric) dipole moment. As we explicitly discuss in Section IV, thermal freeze-out is likely to be dominated by the magnetic dipole interactions, since annihilations mediated by the electric dipole are p-wave suppressed. The situation is reversed for the dark matter (DM) excitations, and in Section V we show that interactions mediated by the electric dipole moment utterly dominate the up-scattering rate.

The analysis of a microscopic origin for the effective interactions in Eq. (2) is beyond the scope of this work, and UV-complete models can be constructed along the lines of e.g. Ref. [17].

A. Fermion Mass Spectrum

The mass eigenstates for the new particles can be found by diagonalizing the fermion mass matrix

$$m_{\rm fermion} = \begin{pmatrix} \delta_\xi & \mu \\ \mu & \delta_\eta \end{pmatrix}\,, \tag{5}$$

which follows from the Lagrangian in Eq. (1). The three mass parameters are in general complex numbers. We always have the freedom to redefine the fields ξ and η to make two mass parameters real and positive. Here, we assume that all the mass parameters are real and positive, and the dipole operators in Eq. (2) are given in the basis where this is the case.

We find it convenient to introduce the parameter

$$\epsilon \equiv \frac{\delta_\xi - \delta_\eta}{2\mu}\,. \tag{6}$$

The exact mass eigenvalues can be expressed as follows

$$m_1 = \mu\sqrt{1+\epsilon^2} - \frac{\delta_\xi + \delta_\eta}{2}\,, \tag{7}$$

$$m_2 = \mu\sqrt{1+\epsilon^2} + \frac{\delta_\xi + \delta_\eta}{2}\,. \tag{8}$$

We are ultimately interested in spectra where the mass splitting, of the order of few keV, is always much smaller than the overall mass scale for the new states. This allows us to express the mass eigenvalues in the $\epsilon \ll 1$ limit

$$m_1 \simeq \mu - \frac{\delta_\xi + \delta_\eta}{2} \equiv m_\chi\,, \tag{9}$$

$$m_2 \simeq \mu + \frac{\delta_\xi + \delta_\eta}{2} \equiv m_\chi + \delta\,. \tag{10}$$

Here, we define m_χ to be the mass of the stable DM particle, and we denote the mass splitting with the excited state by δ. Observationally, δ is a quantity of the utmost importance, as it sets the photon energy for the photon produced in the $\chi_2 \to \chi_1 + \gamma$ decay. The $\epsilon \ll 1$ limit, necessary in our framework to get a small relative mass splitting, can be justified by a hypothetical $U(1)$ symmetry in the UV complete theory that protects the Majorana mass terms $\delta_{\xi,\eta}$. Thus this limit can be quite natural. Strictly speaking, we do not need to forbid Majorana masses to be in this regime of validity, since all we need is the degeneracy between the two Majorana masses in order to have $\delta_\xi - \delta_\eta \ll \mu$. The "line" generated in the $\chi_2 \to \chi_1 + \gamma$ decay is thus at an energy that is effectively a free parameter in our scenario.

[1] The operators $LH\xi$ and $LH\eta$ would be allowed in the absence of the $\mathbb{Z}_2$ symmetry. Here, L and H are the SM lepton and Higgs doublets, respectively. These operators, together with the Majorana mass terms in Eq. (1), would violate lepton number.

The mass eigenstates can also be computed analytically. Here, we report the relevant expressions, once again in the $\epsilon \ll 1$ limit,

$$\chi_1 = \frac{i}{\sqrt{2}}\left(-\xi + \eta\right) \ , \tag{11}$$

$$\chi_2 = \frac{1}{\sqrt{2}}\left(\xi + \eta\right) \ , \tag{12}$$

corresponding to the mass values in Eqs. (9) and (10), respectively.

B. Interactions for Mass Eigenstates

We conclude this Section with the effective interactions in Eq. (2) for the mass eigenstates identified in Eqs. (11) and (12). We express the resulting Lagrangian in terms of the four-component Majorana fermions

$$\psi_1 = \begin{pmatrix} \chi_1 \\ \chi_1^\dagger \end{pmatrix} \ , \qquad \psi_2 = \begin{pmatrix} \chi_2 \\ \chi_2^\dagger \end{pmatrix} \ , \tag{13}$$

and we find

$$\mathcal{L}_{\rm EFT} = -\frac{i}{2\Lambda}\,\overline{\psi_2}\,\Sigma^{\mu\nu}\left(c_M + i\,c_E\gamma^5\right)\psi_1\,F_{\mu\nu} \ . \tag{14}$$

It is straightforward to use the properties of the four-component Majorana spinors in Eq. (13) to check that this Lagrangian is hermitian. Whenever the mass splitting plays a crucial role, as for example in the calculation of the excited state lifetime or the up-scattering rate, we use the interactions as given in Eq. (14). However, to compute the thermal relic density or limits from virtual DM effects, the effect of the mass splitting is completely irrelevant. In these latter cases we perform our calculations in what we call the "Dirac limit", namely when the interactions can be taken as in Eq. (2).

III. EXPERIMENTAL CONSTRAINTS

In this Section we analyze what region of the EFT parameter space is allowed by current experimental bounds. We then study, in the allowed range of parameters, the thermal production of DM and the predicted flux of X-rays from DM excitation in Sec. IV and V, respectively. We do not report here constraints not relevant to our analysis, such as DM-induced contributions to: muon anomalous magnetic moment, electric dipole moments of charged SM fermions, Z-pole observables, invisible B and K meson decays. We checked that all of those constraints are not competitive with the one coming from the electromagnetic coupling running we discuss below [18]. Additionally, searches for mono-photon and mono-jet events at colliders are performed at energy scales above the typical cutoff values we are interested in ($\Lambda \simeq 200\,\text{GeV}$). A correct interpretation of these negative searches would thus require the specification of the underlying UV-complete theory giving the effective interactions in Eq. (2), which is model-dependent and beyond the scope of this work.

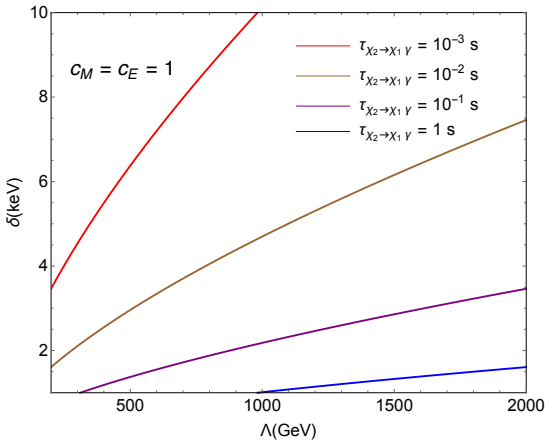

FIG. 1: Lifetime of the excited state decaying to photon through the reaction $\chi_2 \to \chi_1\gamma$. We plot iso-contours in the (Λ, δ) correspondent to different lifetimes. We fix the dipole Wilson coefficients to $c_M = c_E = 1$, for different values the lifetime can be obtained by simply rescaling as in Eq. (16).

A. Big Bang Nucleosynthesis

Light degrees of freedom can alter Big Bang Nucleosynthesis (BBN) and spoil the successful prediction of light elements abundance. We impose two types of BBN constraints:

1. We consider the possibility for DM to freeze-out *after* neutrino decoupling. DM annihilation would then heat the SM plasma with respect to the cosmic neutrino background, *decreasing* the value of the effective relativistic number of degrees of freedom at the BBN epoch $N_{\rm eff}$ [19]. We impose the conservative bound of the DM mass $m_\chi \gtrsim 10\,\text{MeV}$, such that DM freeze-out takes place always before neutrinos decouple.

2. An additional concern pertains the timing for the decay of the excited states χ_2. As will be explained in detail in Sec. IV, thermal freeze-out democratically populates the universe with χ_2 and χ_1 through co-annihilations. The excited state χ_2 has a decay width

$$\Gamma_{\chi_2\to\chi_1\gamma} = \frac{c_M^2 + c_E^2}{8\pi\Lambda^2}\,\frac{(m_2^2 - m_1^2)^3}{m_2^3} \simeq \frac{c_M^2 + c_E^2}{\pi\Lambda^2}\,\delta^3 \ . \tag{15}$$

The first expression is general and does not contain any assumption about the relative size of the mass

splitting. The last expression gives the decay width in the small mass splitting limit, where the masses are given by Eqs. (9) and (10). Interestingly, in such a limit the decay width is controlled only by the mass splitting δ and not by the overall mass scale m_χ. Plugging in typical values for the parameters we are interested in, we find the lifetime $\tau_{\chi_2\to\chi_1\gamma} = \Gamma^{-1}_{\chi_2\to\chi_1\gamma}$ to be typically shorter than the BBN timescale:

$$\tau_{\chi_2\to\chi_1\gamma} = 9.7\times10^{-4}\,\mathrm{s}\,\left(\frac{2}{c_M^2+c_E^2}\right) \times\left(\frac{3.5\,\mathrm{keV}}{\delta}\right)^3\left(\frac{\Lambda}{200\,\mathrm{GeV}}\right)^2 . \tag{16}$$

A thorough exploration of the (Λ,δ) plane is provided in Fig. 1, where we show iso-contours of the excited state lifetime (the scaling for different values of c_M or c_E is entirely trivial). For the parameter range we are interested in this is always below $\tau_{\rm BBN}\simeq 1\,$s and BBN is thus safe.

B. Cosmic Microwave Background

Out-of-equilibrium DM annihilation after freeze-out can change the recombination history and leave an imprint in the CMB spectrum [20–22]. CMB anisotropies bound the DM annihilation strength $\langle\sigma v_{\rm rel}\rangle$, putting an upper limit on the quantity

$$p_{\rm ann} = f_{\rm eff}\,\frac{\langle\sigma v_{\rm rel}\rangle}{m_{\rm DM}} . \tag{17}$$

Here, the efficiency parameter $f_{\rm eff}$ depends on the specific DM annihilation channel. The energy injection takes place over a narrow window of redshift values, thus it is reasonable to approximate $f_{\rm eff}\simeq$ const [22–24]. The values for $f_{\rm eff}$ as a function of the DM mass and for different annihilation channels can be found in Ref. [25]. The latest Planck results on CMB anisotropies [26] give the limit

$$\langle\sigma v_{\rm rel}\rangle < f_{\rm eff}\times 4.1\times10^{-28}\,\mathrm{cm^3 s^{-1}}\left(\frac{m_{\rm DM}}{\rm GeV}\right) . \tag{18}$$

For $m_{\rm DM}$ around 1 GeV, this bound is approximately two orders of magnitude below the value needed at freeze-out $\langle\sigma v_{\rm rel}\rangle_{\rm th} = 3\times10^{-26}\,\mathrm{cm^3 s^{-1}}$ in order to reproduce the observed DM density.

We have three possible DM annihilation final states: leptons, hadrons and photons. The associated Feynman diagrams are shown in Fig. 2. Detailed results for the cross sections can be found in Sec. IV, where we discuss thermal freeze-out. For the purpose of this CMB bound discussion, we limit ourselves to two observations:

1. The annihilation to leptons and hadrons proceeds through an s-channel photon exchange with an off-diagonal vertex. At the time of recombination all the χ_2 have decayed to the stable χ_1, therefore this contribution is absent.

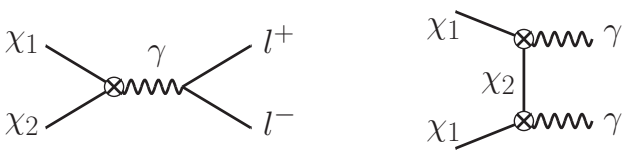

FIG. 2: Feynman diagrams for DM (co)-annihilations. The co-annihilations to leptons (left), as well as the ones to hadrons computed as described in the text, totally dominate the Λ^{-4} suppressed annihilation to photons (right). In both cases, the crossed circle denotes the insertion of the effective magnetic or electric dipole operator.

2. Annihilation to two photons, through the diagram sketched on the right of Fig. 2, is still possible, albeit this channel is suppressed by a double insertion of the dimension-5 dipole operator. This channel has minimal impact on the thermal production of dark matter. As explicitly shown in Eq. (28) in the next Section, this m_χ^2/Λ^2 suppression is quite severe and makes this contribution irrelevant for CMB constraints.

We conclude that CMB limits do not constrain our framework.

C. Direct Detection

The long-range dipole interactions are responsible for quite sizable rates in direct detection (DD) experiments. As is well known [18, 27, 28], this is one of the main reasons why the Wilson coefficients of the dipole operators are severely constrained. However, in our framework as outlined in Sec. II the dipole interactions are off-diagonal and DD can only go through an inelastic channel [29]. Hence DD limits depend on the specific value of the splitting δ, controlling the threshold velocity for the inelastic scattering, and also on the specific experiment because of different energy thresholds to detect the recoil.

We focus our analysis on a mass range $m_\chi\lesssim 1\,$GeV, where the nuclear recoil energy for DM scattering off of nuclei is way below any current experimental threshold, even for the case of elastic scattering. In such a low DM mass range the most promising probe for DD is scattering off of electrons. Xenon10 already put limits on this sub-GeV DM mass range [30, 31], which will be further improved by future experiments [32, 33]. However, these bounds consider the elastic case. The condition to have inelastic scattering reads

$$\delta < \frac{1}{2}\frac{m_\chi m_e}{m_\chi+m_e}\,v^2 \simeq m_e v^2, \tag{19}$$

where δ as above is the mass splitting between the dark sector fermions. While δ is an arbitrary parameter, we are interested in keV emission, thus $\delta\simeq$ keV. For a typical WIMP velocity $v\simeq 10^{-3}$ this condition only applies

to very small mass splitting, on the order of fractions of an eV. Given the mass splitting range of a few keV we are interested in there is no signal in this type of experimental set-up. Thus as long as $m_\chi \lesssim 1\,\text{GeV}$ our model is not constrained by DD exclusion bounds.

D. Electromagnetic Coupling Running

The contact interaction between DM particles and the photon alters the running of the electromagnetic coupling at low energies. This effect can be quantified by computing the one-loop contribution to the photon self-energy accounting for DM particles in the loop. We defer the details of the calculation to App. A.

The running of the electromagnetic coupling is affected as follows:

$$\alpha_{\rm em}(q^2) = \frac{\alpha_0}{1 - C\,\Delta\alpha(q^2)} \ . \tag{20}$$

The fine structure constant α_0 is measured with extremely high precision via the anomalous electron magnetic moment [34]. The function $\Delta\alpha(q^2)$ accounts for only the SM degrees of freedom [35–38], therefore in the absence of the DM particles we would just have $C = 1$. The DM contribution enters C as follows

$$C = 1 + \frac{\Pi^{\rm ren}_{\rm dip}(q^2)}{\Delta\alpha(q^2)} \ , \tag{21}$$

where the renormalized photon self-energy $\Pi^{\rm ren}_{\rm dip}(q^2)$ from virtual DM particles is computed in App. A. Its final expression is given in Eq. (A15). We take the the LEP measurement of the running electromagnetic coupling [39, 40] that are all performed at momentum transfers larger than the DM masses under consideration. For our purposes we can simplify Eq. (A15) in this limit. We find

$$C - 1 = \frac{(-q^2)}{\Delta\alpha(q^2)}\,\frac{c_M^2 + c_E^2}{4\pi^2\Lambda^2}\int_0^1 dx\; x(1-x)\times \ln\left(\frac{m_\chi^2}{m_\chi^2 + (-q^2)x(1-x)}\right) \ . \tag{22}$$

Bhabha-scattering probes the electromagnetic coupling at space-like momentum transfer ($-q^2 > 0$), therefore the above expression is always negative. Consequently, the dipole contribution to C, as parameterized in Eq. (21), is negative and, in our model, we always have $C \leq 1$.

We are ready to compare our theory prediction with LEP data. The analysis in Ref. [40] found the bound

$$C = 1.05 \ \pm\ 0.07_{\rm stat} \ \pm\ 0.14_{\rm syst} \ . \tag{23}$$

We evaluate the DM contribution for $m_\chi = 10\,\text{MeV}$, corresponding to the minimum DM mass we consider, which is also the case when the effect on the running is maximized. Plugging the lowest value of $(-q^2)$ within the range probed by the analysis in Ref. [40], and imposing that we do not violate the bound in Eq. (23) beyond 1σ, we find the following constraints of the combination of Wilson coefficients and the suppression scale

$$\left(c_M^2 + c_E^2\right)\left(\frac{200\,\text{GeV}}{\Lambda}\right)^2 \lesssim 1 \ . \tag{24}$$

For order one Wilson coefficients the running of the electromagnetic coupling requires $\Lambda \gtrsim 200\,\text{GeV}$. The rescaling for different Wilson coefficients is straightforward.

IV. DARK MATTER RELIC DENSITY

In this section we demonstrate that in our model, and for parameter values compatible with the constraints discussed above, the stable DM particle χ_1 can be produced in the early universe through thermal freeze-out. As we have extensively discussed in the previous Section, we are interested in the DM mass range $m_\chi \gtrsim 10\,\text{MeV}$ and a mass splitting $\delta \simeq$ few keV. Thus at the freeze-out epoch, happening when the universe had a temperature approximately $T_f \simeq m_\chi/20$, we expect the excited state χ_2 to be thermally populated; as a result, co-annihilations have to be accounted for. However, since we work in the $\delta \ll m_\chi$ regime, we can treat the (χ_1, χ_2) system as a Dirac fermion with mass m_χ and compute the annihilation cross sections in the "Dirac limit" of Sec. II, namely by using the effective Lagrangian in Eq. (2).

Three possible (co-)annihilation channels keep the DM in thermal equilibrium at early times. Both electric and magnetic dipoles allow the DM to annihilate to lepton pair final states, as shown in the Feynman diagram on the left of Fig. 2. In the non-relativistic limit, appropriate for a cold relic as in our case, we calculate a cross section

$$\sigma_{\chi\chi\,\to\,l^+l^-}\,v_r \simeq \frac{\alpha_{\rm em}}{\Lambda^2}\left[c_M^2 + c_E^2\,\frac{v_r^2}{12}\right]\times \left(1 - \frac{m_l^2}{m_\chi^2}\right)^{1/2}\left(1 + \frac{m_l^2}{2m_\chi^2}\right) \ . \tag{25}$$

As clear from the formula above, annihilation processes mediated by magnetic and electric dipole moments are s- and p-wave processes, respectively. For DM masses above the pion mass, the same interaction vertex with the photon is responsible for annihilation to hadrons. We evaluate this contribution by using the measured value of the observable

$$R_h(\sqrt{s}) = \frac{\sigma_{e^+e^-\,\to\,\text{hadrons}}}{\sigma_{e^+e^-\,\to\,\mu^+\mu^-}} \ . \tag{26}$$

We import numerical values for $R_h(\sqrt{s})$ from the Particle Data Group public webpage [2], which gives the value of

[2] http://pdg.lbl.gov/current/xsect/

this observable for $\sqrt{s} > 0.36\,\text{GeV}$. We fill the gap in the region $2m_\pi \leq \sqrt{s} \leq 0.36\,\text{GeV}$ by using $e^+e^- \to \pi\pi$ scattering data from Ref. [41]. The annihilation cross section to hadrons results in

$$\sigma_{\chi\chi\to\,\text{hadrons}} = \mathcal{R}_h(\sqrt{s}=2m_\chi) \times \sigma_{\chi\chi\to\mu^+\mu^-} \ . \quad (27)$$

A double insertion of dipole operators gives the annihilation to photons shown on the right of Fig. 2. The resulting cross section

$$\sigma_{\chi\chi\to\gamma\gamma}\, v_r \simeq \frac{(c_M^2+c_E^2)^2}{4\pi\,\Lambda^4}\, m_\chi^2 \ , \quad (28)$$

suppressed by the fourth inverse power of Λ, is a subdominant contribution to the total annihilation cross section and it does not play any role at the freeze-out epoch.

The DM number density evolution is described by the Boltzmann equation

$$\frac{dn_\chi}{dt} + 3Hn_\chi = -\langle\sigma v_{\rm rel}\rangle \left(n_\chi^2 - n_\chi^{\rm eq\,2}\right) \ . \quad (29)$$

The thermal average of the cross section for annihilation to leptons in Eq. (25) results in

$$\langle\sigma_{\chi\chi\to l^+l^-}\, v_r\rangle(T) \simeq \frac{\alpha_{\rm em}}{\Lambda^2}\left[c_M^2 + c_E^2\frac{T}{2\,m_\chi}\right]\times \left(1-\frac{m_l^2}{m_\chi^2}\right)^{1/2}\left(1+\frac{m_l^2}{2m_\chi^2}\right) \ , \quad (30)$$

where T is the temperature of the relativistic bath in thermal equilibrium. The total annihilation cross section includes three contributions. Processes with final state electrons, with cross section as in Eq. (30), are always kinematically allowed for the DM mass range we are interested in. Annihilations to muons, with cross section given in Eq. (30), and to hadrons, with cross section obtained through $R_h(\sqrt{s})$ as in Eq. (27), have to be accounted for only if kinematically allowed.

The Boltzmann equation is conveniently solved in terms of the comoving number density $Y_\chi = n_\chi/s$, where s is the entropy density of the relativistic species. Since we are interested in sub-GeV DM, thermal freeze-out is likely to occur during the QCD phase transitions. We take the QCD equation of state, necessary to evaluate the entropy density s and therefore Y_χ, from Ref. [42]. At temperatures much lower than the one at the freeze-out epoch T_f, the comoving density approaches a constant value $Y_\chi^\infty = Y_\chi(T \gg T_f)$. The number and mass density at the present epoch are

$$n_\chi^\infty = 2 \times Y_\chi^\infty s_0 \ , \quad (31)$$
$$\rho_\chi^\infty = m_\chi n_\chi^\infty \ , \quad (32)$$

where we have for the current entropy density [43]

$$s_0 = 2891.2\,\text{cm}^{-3} \ . \quad (33)$$

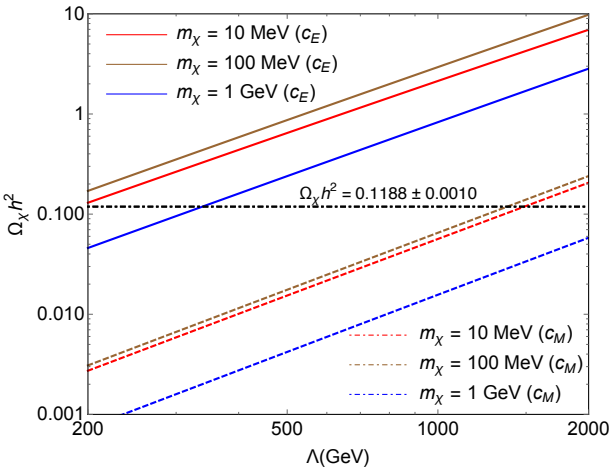

FIG. 3: DM relic density as a function of Λ for three different DM masses (lines with different colors) for purely magnetic dipole interactions ($c_M = 1$, dot-dashed lines) and purely electric dipole interactions ($c_E = 1$, solid lines).

The factor of 2 in Eq. (31) accounts for the fact that we are dealing with a Dirac fermion. Finally, we compute the dark matter contribution to the Ω parameter

$$\Omega_\chi h^2 = \frac{\rho_\chi}{\rho_{\rm cr}/h^2} \ , \quad (34)$$

where the critical density is given by [43]

$$\rho_{\rm cr}/h^2 = 1.05375\times10^{-5}\ \text{GeV}\,\text{cm}^{-3} \ . \quad (35)$$

The output of this calculation has to confront the latest measured value by Planck $\Omega_{\rm DM}h^2 = 0.1188 \pm 0.0010$ [26]. Our final results are summarized in Fig. 3, where we plot the relic density as a function of the suppression scale Λ. We choose three representative value for the DM mass, $m_\chi = (10\,\text{MeV}, 100\,\text{MeV}, 1\,\text{GeV})$, and for each case we compute the relic density for magnetic dipole ($c_M = 1$, dot-dashed lines) and electric dipole ($c_E = 1$, solid lines) interactions. While the figure was produced for $c_{M,E} = 1$, it is straightforward to obtain the relic density for arbitrary Wilson coefficients just by dividing the result of Fig. 3 by $c_{M,E}^2$.

A noteworthy feature of Fig. 3 is that the magnetic dipole lines are always well below the ones for electric dipole moments. This can be understood by looking at Eq. (25), which shows that the latter are p-wave processes and therefore yield a larger relic density.

It is interesting to discuss the dependence on the DM mass. The annihilation cross section for $m_\chi = 10\,\text{MeV}$ and $m_\chi = 100\,\text{MeV}$ is dominated by electron/positron final states and it is approximately the same for both mass values. Despite the two cross sections being identical, the resulting DM relic density is not the same. This residual DM mass dependence is a consequence of the g_* dependence on the freeze-out temperature $T_f \simeq m_\chi/20$, one order of magnitude different in the two cases. The

quite different DM relic density for $m_\chi = 1\,\mathrm{GeV}$ is perhaps more obvious, as hadronic channels are kinematically available, suppressing the total relic density.

To summarize, both magnetic and electric dipole moments can reproduce the observed DM density. For each choice of the DM mass and the suppression scale Λ, all we have to do is to choose c_M or c_E such that $\Omega_\chi h^2 \simeq 0.12$. The relic density for arbitrary values of $c_{M,E}$ is obtained by taking the results shown in Fig. 3 and dividing the predicted value of the relic density in the figure by $c_{M,E}^2$. As we are about to see in the next Section the excitation rate is dominated by c_E, therefore once both couplings are present and comparable we have a remarkable feature of our model: The relic density and the X-ray lines rate are independently controlled by the magnetic and by the electric dipole moments, respectively. For the range of parameters we are interested in, Wilson coefficients for the magnetic dipole in the range $0.1 \lesssim c_M \lesssim 1$ are what is needed to account for the observed DM density.

V. X-RAYS FROM DARK MATTER EXCITATION

In this Section we evaluate the predicted flux of X-ray photons originating from the excitation process

$$\chi_1\, f \;\rightarrow\; \chi_2\, f \;, \tag{36}$$

followed by the decay process

$$\chi_2 \;\rightarrow\; \chi_1 \gamma \;. \tag{37}$$

The Feynman diagram for the up-scattering is shown in Fig. 4. The particle f is a SM fermion present in the plasma. For simplicity we consider contributions from electrons and protons and neglect that from heavier elements. The excited state χ_2 is quite short-lived compared to cosmological timescales, as explicitly shown in Eq. (16). Hence once the DM up-scatters off of a plasma fermion into the χ_2 particle, the subsequent decay back to the stable DM particle χ_1 and the consequent emission of a X-ray photon are effectively instantaneous. The final state photon energy is equal to the mass splitting between the two fermion states (up to corrections due to the velocity distribution of the plasma fermion and of the dark matter, as discussed below):

$$E_\gamma = \frac{m_{\chi_2}^2 - m_{\chi_1}^2}{2 m_{\chi_2}} \simeq \delta \;. \tag{38}$$

The predicted X-ray flux in our model resulting from DM excitation and decay reads

$$\Phi = \kappa_{\rm eff}\, \langle \sigma v_{\rm rel} \rangle \;, \tag{39}$$

where $\kappa_{\rm eff}$ is the integral along the line of sight and over the appropriate (solid) angular region of interest $\Delta\Omega$ (corresponding to angles of aperture of around 6 arcmin for X-ray observations, unless otherwise specified) of the product of the plasma particles' number density $n_f(\vec{r})$ times the dark matter number density $n_{\rm DM} = \rho_{\rm DM}(r)/m_\chi$, and has units of cm^{-5},

$$\kappa_{\rm eff} \equiv \int_{\Delta\Omega} d\Omega \int_{\rm l.o.s.} dl \; n_f(\vec{r}(l,\Omega))\, n_{\rm DM}(\vec{r}(l,\Omega)), \tag{40}$$

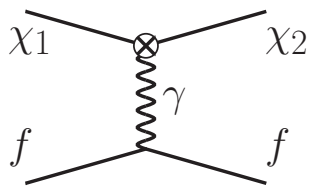

FIG. 4: Feynman diagram for DM inelastic up-scattering. Here, f can be either an electron or a proton. The crossed circle denotes the insertion of the effective magnetic or electric dipole operator.

where f is either a proton or an electron. The thermally averaged cross section is defined as

$$\langle \sigma v_{\rm rel} \rangle = \int d^3 v_\chi d^3 v_f \; f_{\rm DM}(v_\chi) f_f(v_f)\; \sigma v_{\rm rel} \;, \tag{41}$$

where $f_{\rm DM}$ and f_f are the normalized phase space distribution functions of the DM particle and the SM fermion, respectively. We consider for our analysis normalized Gaussian distributions

$$f_i(v_i) = \frac{a_i^{3/2}}{\pi^{3/2}} e^{-a_i v_i^2} \;. \tag{42}$$

where $i = \chi, f$. As derived in App. B, the thermal average can be expressed in a very simple form, namely

$$\langle \sigma v_{\rm rel} \rangle = \int_{v_{\rm rel}^{\rm min}}^{\infty} dv_{\rm rel}\; \sigma(v_{\rm rel})\; \mathcal{F}(v_{\rm rel}). \tag{43}$$

The integration is over the relative velocity in the CM frame of the inelastic scattering in Eq. (36). Such a collision can only take place for relative velocity values above the kinematic threshold

$$v_{\rm rel}^{\rm min} = \left(\frac{m_\chi + m_f}{m_\chi m_f}\, 2\delta \right)^{1/2} . \tag{44}$$

The integrand in Eq. (43) is the product of the total inelastic cross section and a "Kernel function"

$$\mathcal{F}(v_{\rm rel}) = \frac{4 v_{\rm rel}^3}{\pi^{1/2}} \left(\frac{a_\chi a_f}{a_\chi + a_f} \right)^{3/2} \exp\left(- \frac{a_\chi a_f}{a_\chi + a_f}\, v_{\rm rel}^2 \right) . \tag{45}$$

Here, the coefficients $a_{\chi,f}$ denotes the width of the thermal distribution in Eq. (42). In particular, for the two cases we are interested in we have, in natural units,

$$a_\chi = \frac{1}{v_0^2} \simeq 10^6 \;, \tag{46}$$

$$a_f = \frac{m_f}{2 T_f} \;. \tag{47}$$

A. General Features of the Rate

Before discussing the two cases we are interested in, namely the Perseus cluster of galaxies and the Galactic Center, we point out a few general facts about the X-ray line rates in our framework. The above discussion is very general and does not assume any specific type of interaction mediating the inelastic collision in Eq. (36). We specialize now on the dipole interactions introduced in Section II. We are considering an inelastic collision, therefore the cross section has to be computed by using the Lagrangian for mass eigenstates given in Eq. (14).

The expression for the up-scattering cross section is quite involved. It is helpful to look at the limiting case when the mass splitting is negligible [18]:

$$\frac{d\sigma}{d\Omega} = \frac{c_M^2\, e^2}{16\pi^2\Lambda^2}\, \frac{1+\frac{m_\chi(m_\chi-2m_f)}{(m_\chi+m_f)^2}\sin^2(\theta/2)}{\sin^2(\theta/2)}\,, \tag{48}$$

$$\frac{d\sigma}{d\Omega} = \frac{c_E^2\, e^2}{16\pi^2\Lambda^2}\, \frac{1}{v_{\rm rel}^2\,\sin^2(\theta/2)}\,, \tag{49}$$

for magnetic and electric dipole moments, respectively. Both expressions are divergent at small θ. Furthermore, the cross section for the process mediated by the dipole is also divergent at small relative velocities. The introduction of a finite mass splitting regularizes all the above divergences and our final results are thus finite. The usefulness of Eqs.(48) and (49) is in the small velocity behavior: since we are interested in the non-relativistic regime, we expect the electric dipole contribution to dominate the total excitation rate.

This can be quantified by performing the full computation of the cross section and evaluating the thermal average as prescribed by Eq. (43). Giving the scaling of our dipole interactions in Eq. (14), the thermal average can be parameterized as follows:

$$\langle\sigma v_{\rm rel}\rangle = \frac{e^2}{\Lambda^2}\left[c_M^2\,\Sigma_M(m_\chi,\delta) + c_E^2\,\Sigma_R(m_\chi,\delta)\right]\,. \tag{50}$$

In this expression we assume the other parameters (i.e. the DM dispersion velocity, fermion mass and temperature) to be fixed, and therefore the functions $\Sigma_{M,E}$ to only depend on the DM mass and on the mass splitting.

For the sole purpose of illustration we fix

$$\begin{aligned} &v_0 = 10^{-3}c\,,\\ &m_f = (511\,\text{keV}, 938\,\text{MeV})\,, \qquad T_f = 5\,\text{keV}\,. \end{aligned} \tag{51}$$

The two different values of m_f correspond to electrons and protons, respectively. For this choice of parameters, we plot in Fig. 5 the functions $\Sigma_{M,E}$ defined in Eq. (50) as a function of the DM mass for $\delta = 1\,\text{keV} < T_f$. In particular, we have $\delta < T_f$ and the plasma kinetic energy is able to easily excite χ_1 to the heavier state χ_2.

As correctly anticipated above, rates from electric dipoles are always larger than those from magnetic dipoles. This effect is due to the small velocity singularity in Eq. (49), regularized now by the finite mass splitting, but still capable of enhancing by orders of magnitude the total rate. Another interesting feature of Fig. 5 is the drastically different behavior between scattering off of electrons and protons. Scattering off of electrons is independent on m_χ for the DM mass range under investigation. In contrast, scattering off of protons is much more efficient for larger DM masses. This is a combination of two effects. The Maxwell-Boltzmann suppression for the proton is more severe, as it can be easily seen from the explicit expression for $\mathcal{F}(v_{\rm rel})$ in Eq. (45). However, Eq. (45) is not sensitive to the DM mass, which enters only by setting the threshold velocity. This kinematical limit is given in Eq. (44), where the reduced mass of the DM-fermion system appears in the denominator. Therefore, for m_χ below the proton mass the threshold velocity is just too high to be thermally accessible.

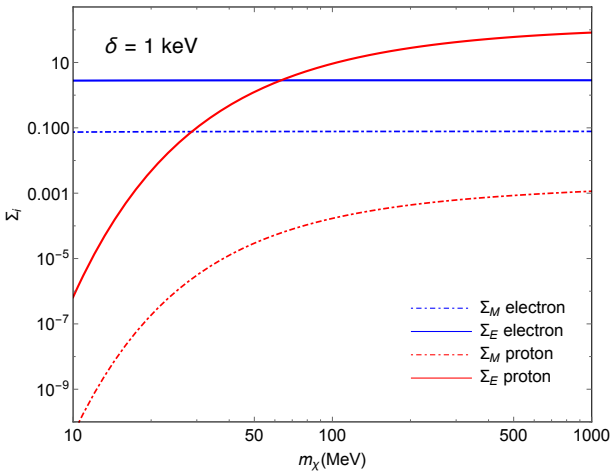

FIG. 5: Functions $\Sigma_{M,E}$ defined as in Eq. (50) as a function of the DM mass. The parameters are fixed as in Eq. (51) and the mass splitting is set to $\delta = 1\,\text{keV}$. We show results for magnetic and dipole moments with dot-dashed and solid lines, respectively. Moreover, we separate the contribution from electrons (blue lines) and protons (red lines).

B. Perseus

We focus here on the first of two illustrative cases, the Perseus cluster. The rate of dark matter excitation by the interstellar plasma is given by Eq. (39). The effective plasma-times-dark matter number density $\kappa_{\rm eff}$ as defined in Eq. (40) is calculated following Ref. [14], for the observationally relevant angular region. We use a Navarro-Frenk-White density profile [44] for the dark matter density distribution in the Perseus cluster of the form

$$\rho_{\rm DM}(r) = \frac{\rho_0}{\left(\frac{r}{R_s}\right)\left(1+\frac{r}{R_s}\right)^2}\,. \tag{52}$$

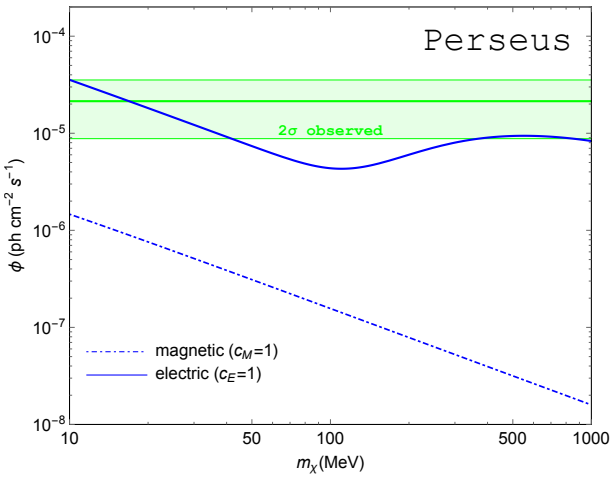

FIG. 6: Predicted rate of X-ray photons from the Perseus cluster as a function of the DM mass. We show contributions from both magnetic (dot-dashed lines) and electric (solid lines). Here, we set $\delta = 3.5\,\text{keV}$ and $\Lambda = 200\,\text{GeV}$. The green band indicates the 2σ region for the observed 3.5 keV line flux [5].

The parameters are derived using the results of Ref. [45] with the concentration-mass relation as quoted in Ref. [46],

$$R_s = 445\,\text{kpc}\ , \tag{53}$$

$$\rho_0 = 0.0217\,\text{GeV/cm}^3\ . \tag{54}$$

For the electron density we use the following double β-function density profile [47]

$$n_e(r) = \frac{3.9\times10^{-2}\ \text{cm}^{-3}}{\left(1+\left(\frac{r}{80\ \text{kpc}}\right)^2\right)^{1.8}} + \frac{4.05\times10^{-3}\ \text{cm}^{-3}}{\left(1+\left(\frac{r}{280\ \text{kpc}}\right)^2\right)^{0.87}}\ . \tag{55}$$

The calculation of the integral in Eq. (40) gives, for an angular region between angles of $1'$ and $12'$ of the center of the cluster as used in Ref. [5],

$$\kappa_{\text{eff}}^{\text{Perseus}} \simeq 1.06\times10^{18}\ \left(\frac{10\,\text{MeV}}{m_\chi}\right)\ \text{cm}^{-5}\ . \tag{56}$$

We fix the virial temperature to [45]

$$T_f|_{\text{Perseus}} = 6.8\,\text{keV}\ . \tag{57}$$

Moreover, we fix the mass splitting to $\delta = 3.5\,\text{keV}$ and the suppression scale to $\Lambda = 200\,\text{GeV}$ (the rescaling of the rates with Λ is straightforward).

The results for the fluxes are shown in Fig. 6, where we also include the 3.5 keV line flux as quoted in Ref. [5]. The magnetic contribution is negligible. The flux of the X-ray line from electric dipole interactions has an interesting dependence on m_χ: At low DM mass, $m_\chi \simeq 10\,\text{MeV}$, the rate is dominated by scattering off of electrons and it falls as m_χ^{-1} because of the depletion in the DM number density, see Eq. (56). As the DM mass becomes larger than $m_\chi \simeq 100\,\text{MeV}$, scattering off of protons becomes efficient for the reasons explained at the end of Section V A. This induces a temporary rise in the flux, which eventually starts falling again because of the number density depletion once the proton up-scattering cross section reaches its asymptotic limit.

C. Galactic Center

We perform an analogous analysis for the X-ray data from the Galactic center (GC) Ref. [6]. In this case we conservatively consider a cored Burkert profile [48] for the dark matter density (other possibilities are discussed below)

$$\rho_{\text{DM}}(r) = \frac{\rho_0\ R_s^3}{(r+R_s)\,(r^2+R_s^2)}\ . \tag{58}$$

We set $\rho_0 = 2.9\ \text{GeV/cm}^3$ and $R_s = 6.0\ \text{kpc}$ [14]. The interstellar gas density is taken to be the sum of the "thick" and "thin" disk components of Ref. [49], with the parameters provided in Tab. 2 and 3 in Ref. [49]. We do not include the contribution from the central molecular zone, as the contribution from similar molecular clouds is absent from the modeling of the plasma density for Perseus.

For the GC plasma temperature we consider a multi-temperature model consisting of an admixture of two different temperatures: $T_f = 1\,\text{keV}$ with density 4/5 of the total, and the remaining 1/5 with temperature $T_f = 7\,\text{keV}$ [6]. We checked that employing a single-temperature model does not affect our results significantly. The resulting normalization factor for the excitation rate from the Galactic center is

$$\kappa_{\text{eff}}^{\text{GC}} = 7.82\times10^{18}\ \left(\frac{10\,\text{MeV}}{m_\chi}\right)\ \text{cm}^{-5}. \tag{59}$$

We present results for the photon flux and comparison with observation (assuming no contribution to the 3.5 keV line from, e.g., K), as detected and reported in Ref. [6], in Fig. 7.

We also considered other choices for the dark matter density profile. For example, employing a Navarro-Frenk-White density profile [44] the predicted rate of X-rays from excitation would be around one order of magnitude larger than with a Burkert profile. This could still be made consistent with observations from Perseus if a fraction of the 3.5 X-ray there were associated with emission from e.g. K XVIII de-excitation.

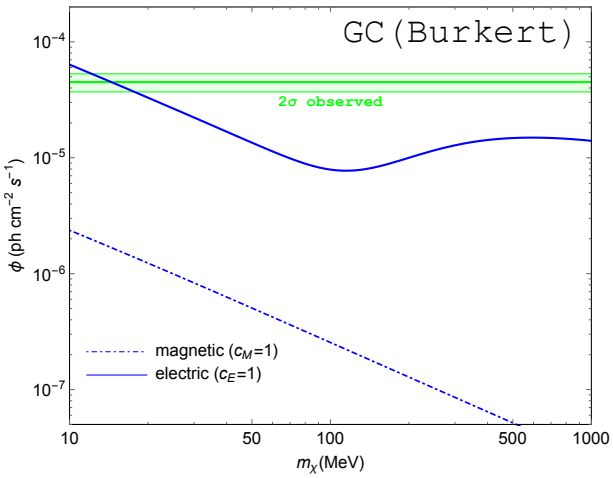

FIG. 7: Predicted rate of X-ray photons from the Galactic Center as a function of the DM mass, with the 2-σ range for the detected line flux at energies around 3.5 keV Ref. [6]. Conventions are as in Fig. 6; we again set $\delta = 3.5\,\text{keV}$ and $\Lambda = 200\,\text{GeV}$.

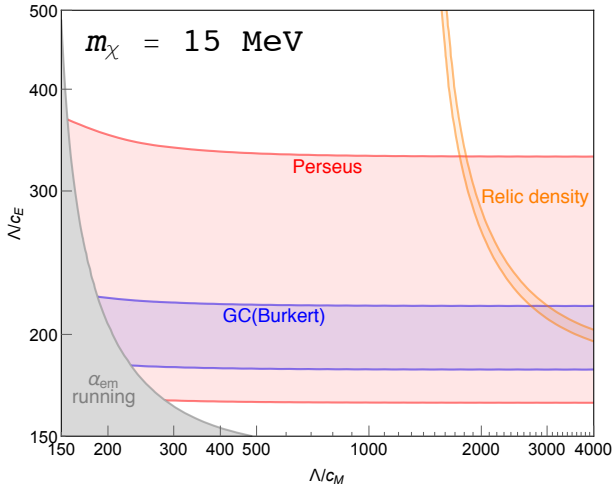

FIG. 8: Summary plot for $m_\chi = 15\,\text{MeV}$.

VI. DISCUSSION AND CONCLUSIONS

Fig. 6 and 7 illustrate that our model predicts X-ray fluxes from dark matter thermal plasma excitations from the Galactic center and from Perseus compatible with observations for a range of dark matter masses. For the choice $c_M = c_E = 1$ and $\Lambda = 200$ GeV, this mass range is in the 10-20 MeV mass range; larger values for c_E/Λ would shift the preferred mass range to larger masses; the same would be true if a fraction of the observed X-ray flux at 3.5 keV were to be attributed to other mechanisms than the one under consideration, for example from K ions.

Fig. 8 examines, for a mass $m_\chi = 15$ MeV, the parameter space in the $(\Lambda/c_M, \Lambda/c_E)$ plane compatible with X-ray observations *and* producing a thermal relic dark matter abundance in accordance with the observed cosmological dark matter density. The red shaded region is compatible with the observed flux from Perseus, and the blue region with the flux detected from the Galactic center (assuming a Burkert density profile, and assuming the whole 3.5 keV line flux is associated only with dark matter de-excitations). Finally, the orange region is compatible with dark matter being entirely produced as a thermal relic, and the grey region is excluded by the running of the electromagnetic coupling.

We thus find that there exists theory parameter space where our models features a thermal relic that explains the 3.5 keV line observations. The preferred ratio of the Wilson coefficients, for the mass choice we made, is $c_E/c_M \sim 10-15$, which is not incompatible with generic theoretical expectations for the two parameters being in a similar ballpark.

We emphasize once again that while our model *does* provide a consistent explanation to the observational landscape of the 3.5 keV line for thermal relic dark matter, the mass splitting between the two dark sector fermions is a free parameter. As a result, lines could be produced in principle at any energies below the typical temperatures of the plasma (few keV). This opens up a brand new observational window to search for signals from the dark sector. The predicted signals are unique in three respects:

1. The *line-shape* is peculiar: it is a geometric product of the width of the dark matter and of the thermal plasma velocity distribution (see Eq. (45)); with sufficient energy resolution, such as that expected for the newly launched Hitomi X-ray satellite [16], it will be thus possible to discriminate this mechanism against other sources of X-ray lines such as dark matter decay or plasma de-excitation lines;

2. The *morphology* of the predicted emission depends on a unique line-of-sight integral of the product of the plasma density times the dark matter density, in contrast with other models where the signal depends on the dark matter density, density squared, or on magnetic fields;

3. The *brightest predicted targets* depend not only on the integral mentioned above, but also on the target's temperature: depending on the dark sector mass splitting, large temperatures might be needed to excite the heavier particle to significant levels; As a result, colder targets might be significantly dimmer than hotter ones.

In summary, we have proposed and studied in detail a simple model for the dark sector that offers novel and unique detection prospects. The model consists of two (gauge) "sterile" Weyl fermions, odd under a $\mathbb{Z}_2$ symmetry, and coupled to the Standard Model via an effective inelastic magnetic and electric dipole operator. The

model effectively contains four parameters: the suppression scale for the two dipole operators, and the masses of the two fermions.

We scrutinized in great detail the phenomenology of the model, and concluded that (i) the mass of the lightest state is constrained by cosmology to be heavier than about 10 MeV, and (ii) the strongest constraint on the scale of the effective dipole operators is from corrections to the running of the electromagnetic coupling. We then studied the thermal relic density of the dark matter, and demonstrated that it is driven by the *magnetic* dipole term and can easily match the observed universal dark matter density for a broad range of dark matter masses. The model predicts significant production of the heavier fermion from inelastic collision of the lighter (dark matter) fermion with the thermal plasma in galaxies or clusters of galaxies. This up-scattering rate is driven by the *electric* dipole term, and is predicted to source a bright, detectable line through the decay of the heavier fermion to the lighter fermion and a quasi-monochromatic photon.

Remarkably, there exist at least *three independent unique observational handles* that could discriminate this scenario from other background processes producing lines or other new physics scenarios: the line's width, its morphology, and the (predictable) dependence on the target's temperature. The energy of the predicted line is essentially a free parameter of the theory, as long as it is at energies comparable or lower than the typical plasma temperature of a given astrophysical target. This model opens a new exciting window for the search of the first non-gravitational manifestation of dark matter as a particle.

Acknowledgments

FD is grateful to Howard Haber, Jeremy Mardon and Duccio Pappadopulo for useful discussions. SP is grateful to Eric Carlson for help and consultations on plasma density models. FD, SP and TS are partly supported by the U.S. Department of Energy grant number DE-SC0010107. TS is furthermore supported by a Feodor-Lynen research fellowship sponsored by the Alexander von Humboldt foundation.

Appendix A: One-loop Running of the Electromagnetic Coupling

In this Appendix we provide the calculation of the one-loop electromagnetic coupling running. We evaluate the contribution to the photon self-energy sketched in Fig. 9 in the "Dirac limit" (e.g. by using Eq. (2)), justified since we consider $\delta \ll m_\chi$. The photon self-energy results in

$$i\,\Pi^{\mu\nu}_{\rm dip}(q) = -\frac{1}{\Lambda^2}\int \frac{d^dk}{(2\pi)^d}\,\frac{{\rm Tr}\left[(\not{k}+m_\chi)\,q_\alpha\Sigma^{\alpha\mu}(c_M+ic_E\gamma^5)\left(\not{k}+\not{q}+m_\chi\right)q_\beta\Sigma^{\beta\nu}(c_M+ic_E\gamma^5)\right]}{(k^2-m_\chi^2)((k+q)^2-m_\chi^2)}\,, \tag{A1}$$

where we regularize the UV behavior by computing the loop integral in d space-time dimensions. The calculation proceeds by introducing the Feynman parameters and performing the change of integration variable $l = k + qx$

$$i\,\Pi^{\mu\nu}_{\rm dip}(q) = -\frac{1}{\Lambda^2}\int_0^1 dx\int \frac{d^dl}{(2\pi)^d}\,\frac{{\rm Tr}\left[\left(\not{l}-\not{q}x+m_\chi\right)q_\alpha\Sigma^{\alpha\mu}(c_M+ic_E\gamma^5)\left(\not{l}+\not{q}(1-x)+m_\chi\right)q_\beta\Sigma^{\beta\nu}(c_M+ic_E\gamma^5)\right]}{(l^2-\Delta)^2}\,, \tag{A2}$$

where we also introduced

$$\Delta = m_\chi^2 - q^2x(1-x)\,. \tag{A3}$$

All the terms with an odd power of l in the numerator of Eq. (A2) vanish by parity consideration. The Dirac trace of the surviving terms is straightforward. Consistently with electromagnetic gauge invariance, the expression we find is transverse, $\Pi^{\mu\nu}_{\rm dip}(q) = \left(q^2g^{\mu\nu}-q^\mu q^\nu\right)\Pi_{\rm dip}(q^2)$, where the quantity $\Pi(q)$ results in

$$\Pi_{\rm dip}(q^2) = i\frac{4}{\Lambda^2}\int_0^1 dx\int\frac{d^dl}{(2\pi)^d}\left[\frac{(c_M^2+c_E^2)q^2x(1-x)+(c_M^2-c_E^2)m_\chi^2}{(l^2-\Delta)^2}+\frac{\left(1-\frac{4}{d}\right)(c_M^2+c_E^2)\,l^2}{(l^2-\Delta)^2}\right]\,. \tag{A4}$$

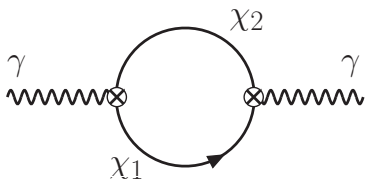

FIG. 9: Feynman diagram for the one-loop photon propagator. The crossed circle denotes the insertion of the effective magnetic or electric dipole operator.

The term proportional to l^2 vanishes in $d = 4$, and it can be explicitly checked that it has no $d = 4$ pole in dimensional regularization. However, it has a finite piece that we keep in our analysis.

The next step is to compute the loop integral in Eq. (A4) in $d = 4 - 2\epsilon$ space-time dimensions. The two terms can be evaluated by using the general results

$$\int \frac{d^d l}{(2\pi)^d} \frac{1}{(l^2 - \Delta)^2} = i\, \mathfrak{L}_0 \ , \tag{A5}$$

$$\int \frac{d^d l}{(2\pi)^d} \frac{l^2}{(l^2 - \Delta)^2} = i\, \frac{\Delta}{1 - 2/d}\, \mathfrak{L}_0 \ . \tag{A6}$$

Here, we define

$$\mathfrak{L}_0 \equiv \frac{\Gamma(2 - d/2)}{(4\pi)^{d/2}\, \Delta^{2-d/2}} \ , \tag{A7}$$

with $\Gamma(x)$ the Euler function. Upon Taylor-expanding around 4 dimensions, with expansion parameter $\epsilon = (4 - d)/2$, we find

$$\Gamma(2 - d/2) = \Gamma(\epsilon) = \frac{1}{\epsilon} - \gamma_E + \mathcal{O}(\epsilon) \ , \tag{A8}$$

where $\gamma_E \simeq 0.577$ is the Euler-Mascheroni constant. Therefore in $d = 4 - 2\epsilon$ dimensions, up to $\mathcal{O}(\epsilon)$ terms, the quantity $\mathfrak{L}_0$ defined in Eq. (A7) reads

$$\mathfrak{L}_0 = \frac{1}{16\pi^2} \left[\frac{1}{\epsilon} + \ln\left(\frac{4\pi\, e^{-\gamma_E}}{m_\chi^2 - q^2 x(1-x)} \right) \right] \ . \tag{A9}$$

Here, we have restored the explicit functional form for Δ as given in Eq. (A3).

After computing the loop integral as we have just described, the photon self-energy in Eq. (A4) becomes

$$\begin{aligned} \Pi_{\rm dip}(q^2) = &-\frac{1}{\epsilon}\, \frac{1}{4\pi^2\Lambda^2} \left[(c_M^2 + c_E^2) \frac{q^2}{6} + (c_M^2 - c_E^2) m_\chi^2 \right] + \frac{(c_M^2 + c_E^2)}{4\pi^2\Lambda^2} \left(m_\chi^2 - \frac{1}{6} q^2 \right) \\ &- \frac{1}{4\pi^2\Lambda^2} \int_0^1 dx \left[(c_M^2 + c_E^2) q^2 x(1-x) + (c_M^2 - c_E^2) m_\chi^2 \right] \ln\left(\frac{4\pi\, e^{-\gamma_E}}{m_\chi^2 - q^2 x(1-x)} \right) \ , \end{aligned} \tag{A10}$$

where we only keep terms surviving after the $\epsilon \to 0$ limit.

The one-loop photon self-energy in Eq. (A10) has a $1/\epsilon$ divergence that needs to be renormalized. The pole proportional to the squared DM mass is taken care of by a renormalization of the photon kinetic term, as it happens in regular QED. However, the pole proportional to q^2 requires the introduction of a new dimension 6 operator

$$\mathcal{O}_6 = \frac{1}{4} F^{\mu\nu} \Box F_{\mu\nu} \ . \tag{A11}$$

The renormalized photon self-energy is given by the one-loop contribution in Eq. (A10) summed to the two infinite counterterms mentioned above

$$\Pi_{\rm dip}^{\rm ren}(q^2) = \Pi_{\rm dip}(q^2) - \delta_4 - \delta_6\, q^2 \ , \tag{A12}$$

where δ_4 and δ_6 are the counterterms for the photon kinetic term and the dimension 6 operator in Eq. (A11), respectively.

The next step is to go from the full self-energy in Eq. (A12) to the running electromagnetic coupling. We compare our prediction with Bhabha-scattering data. As is well known [50], the running coupling is given by

$$\alpha_{\rm em}(q^2) = \frac{\alpha_0}{1 - \Pi(q^2)} \ , \tag{A13}$$

where α_0 is the fine structure constant and $\Pi(q^2)$ is the full photon self-energy, which is given by the sum of the SM contribution and the renormalized dipole contribution in Eq. (A12). The SM contribution to the QED vacuum polarization is well known [35–38]. All we have left to do is to add the DM contribution, but before doing so we have to fix the counterterms δ_4 and δ_6 appearing in Eq. (A12). We start from fixing δ_4, and we do that by requiring that $\alpha_{\rm em}(q^2 = 0) = \alpha_0$, or in other words we choose δ_4 to make sure that $\Pi_{\rm dip}^{\rm ren}(q^2 = 0) = 0$ as follows

$$\Pi^{\rm ren}_{\rm dip}(q^2) = -\,q^2\frac{c_M^2+c_E^2}{24\pi^2\Lambda^2}\left(\frac{1}{\epsilon}+1\right) - \frac{(c_M^2-c_E^2)m_\chi^2}{4\pi^2\Lambda^2}\int_0^1 dx\ln\left(\frac{m_\chi^2}{m_\chi^2-q^2x(1-x)}\right) - q^2\frac{c_M^2+c_E^2}{4\pi^2\Lambda^2}\int_0^1 dx\,x(1-x)\ln\left(\frac{4\pi\,e^{-\gamma_E}}{m_\chi^2-q^2x(1-x)}\right) - \delta_6\,q^2\ . \tag{A14}$$

The renormalization condition at $q^2 = 0$ cannot fix the counterterm δ_6, because its effects vanish in the static limit. Thus in order to fix δ_6 we need another experimental input. At energy scales much smaller than the DM mass we consider, namely $-q^2 \ll (10\,\mathrm{MeV})^2$, the DM particles in the loop cannot affect the gauge coupling running. We evaluate Eq. (A13) in such regime, and find the δ_6 we need in order to have only the SM contribution. The final renormalized DM contribution to the photon self-energy reads

$$\Pi^{\rm ren}_{\rm dip}(q^2) = -m_\chi^2\frac{(c_M^2-c_E^2)}{4\pi^2\Lambda^2}\int_0^1 dx\ln\left(\frac{m_\chi^2}{m_\chi^2-q^2x(1-x)}\right) - q^2\frac{c_M^2+c_E^2}{4\pi^2\Lambda^2}\int_0^1 dx\,x(1-x)\ln\left(\frac{m_\chi^2}{m_\chi^2-q^2x(1-x)}\right)\ . \tag{A15}$$

Appendix B: A Simple Formula for the Thermal Average of the Excitation Rate

In this Appendix we derive the simple expression for the thermal average given in Eq. (43). We start from the definition in Eq. (41), which involves six integrals. It is convenient to change integration variables

$$\boldsymbol{V} = \frac{\boldsymbol{v}_\chi + \boldsymbol{v}_f}{2}\ , \tag{B1}$$

$$\boldsymbol{v}_{\rm rel} = \boldsymbol{v}_\chi - \boldsymbol{v}_f\ . \tag{B2}$$

The up-scattering cross section is a Lorentz-invariant quantity that depends only on the CM energy $\sqrt{s}$ of the collision. In the non-relativistic limit we have

$$s = \left(m_\chi + m_f + \frac{1}{2}\frac{m_\chi m_f}{m_\chi+m_f}v_{\rm rel}^2\right)^2\ , \tag{B3}$$

therefore the cross section can only depend on the absolute value of the relative velocity between the two particles, as correctly reproduced in Eq. (43).

The inelastic collision initial state is characterized by three quantities: the magnitude of the two velocities and the angle between them. The integration in the new variables can be performed in polar coordinates, i.e.

$$d^3V d^3v_{\rm rel} \ \rightarrow\ 4\pi\times 2\pi\times dV\,dv_{\rm rel}\,d\cos\gamma\,V^2v_{\rm rel}^2\ , \tag{B4}$$

where we define γ as the angle between $\boldsymbol{V}$ and $\boldsymbol{v}_{\rm rel}$. Upon expressing the thermal average as in Eq. (43), the function $\mathcal{F}(v_{\rm rel})$ reads

$$\mathcal{F}(v_{\rm rel}) \equiv 8\pi^2 v_{\rm rel}^3\int_0^\infty dV\,V^2\int_{-1}^1 d\cos\gamma\ \times\ f_{\rm DM}(V,v_{\rm rel},\cos\gamma)f_f(V,v_{\rm rel},\cos\gamma)\ . \tag{B5}$$

The distribution functions can be easily expressed as a function of V and $v_{\rm rel}$ by using the relations

$$v_\chi^2 = \boldsymbol{v}_\chi\cdot\boldsymbol{v}_\chi = V^2 + \frac{v_{\rm rel}^2}{4} + Vv_{\rm rel}\cos\gamma\ , \tag{B6}$$

$$v_f^2 = \boldsymbol{v}_f\cdot\boldsymbol{v}_f = V^2 + \frac{v_{\rm rel}^2}{4} - Vv_{\rm rel}\cos\gamma\ . \tag{B7}$$

All we have to do to get to Eq. (45) is to introduce the explicit form of the distribution functions. We integrate over the angle γ by using the relation

$$\int_{-1}^1 d\cos\gamma\exp\left[-\left(a_\chi-a_f\right)Vv_{\rm rel}\cos\gamma\right] = 2\,\frac{\sinh\left[\left(a_\chi-a_f\right)Vv_{\rm rel}\right]}{\left(a_\chi-a_f\right)Vv_{\rm rel}}\ , \tag{B8}$$

and consequently the function $\mathcal{F}(v_{\rm rel})$ results in

$$\mathcal{F}(v_{\rm rel}) = \frac{16v_{\rm rel}^2\,a_\chi^{3/2}a_f^{3/2}\,\exp\left[-\left(a_\chi+a_f\right)\frac{v_{\rm rel}^2}{4}\right]}{\pi\left(a_\chi-a_f\right)}\times \int_0^\infty dV\,V\exp\left[-\left(a_\chi+a_f\right)V^2\right]\times \sinh\left[\left(a_\chi-a_f\right)Vv_{\rm rel}\right]\ . \tag{B9}$$

Finally, the integration over V can be performed by using

$$\int_0^\infty dV\,V\,\exp\left[-\alpha V^2\right]\,\sinh\left[\beta V\right] = \frac{\pi^{1/2}}{4}\frac{\beta}{\alpha^{3/2}}\exp\left[\frac{\beta^2}{4\alpha}\right]\ , \tag{B10}$$

with the final expression for $\mathcal{F}(v_{\rm rel})$ as given in Eq. (45).

[1] J. L. Feng et al., in *Community Summer Study 2013: Snowmass on the Mississippi (CSS2013) Minneapolis, MN, USA, July 29-August 6, 2013* (2014), 1401.6085, URL `https://inspirehep.net/record/1278570/files/arXiv:1401.6085.pdf`.

[2] S. Profumo and P. Ullio (2010), 1001.4086.

[3] P. W. Graham, I. G. Irastorza, S. K. Lamoreaux, A. Lindner, and K. A. van Bibber, Ann. Rev. Nucl. Part. Sci. **65**, 485 (2015), 1602.00039.

[4] E. Carlson and S. Profumo, Phys. Rev. **D92**, 063003 (2015), 1504.04782.

[5] E. Bulbul, M. Markevitch, A. Foster, R. K. Smith, M. Loewenstein, and S. W. Randall, Astrophys. J. **789**, 13 (2014), 1402.2301.

[6] T. E. Jeltema and S. Profumo, Mon. Not. Roy. Astron. Soc. **450**, 2143 (2015), 1408.1699.

[7] A. Boyarsky, O. Ruchayskiy, D. Iakubovskyi, and J. Franse, Phys. Rev. Lett. **113**, 251301 (2014), 1402.4119.

[8] T. Jeltema and S. Profumo (2014), 1411.1759.

[9] D. Malyshev, A. Neronov, and D. Eckert, Phys. Rev. **D90**, 103506 (2014), 1408.3531.

[10] T. E. Jeltema and S. Profumo (2015), 1512.01239.

[11] M. E. Anderson, E. Churazov, and J. N. Bregman, Mon. Not. Roy. Astron. Soc. **452**, 3905 (2015), 1408.4115.

[12] R. Adhikari et al. (2016), 1602.04816.

[13] K. J. H. Phillips, B. Sylwester, and J. Sylwester, Astrophys. J. **809**, 50 (2015).

[14] E. Carlson, T. Jeltema, and S. Profumo, JCAP **1502**, 009 (2015), 1411.1758.

[15] M. Cicoli, J. P. Conlon, M. C. D. Marsh, and M. Rummel, Phys. Rev. **D90**, 023540 (2014), 1403.2370.

[16] T. Kitayama, M. Bautz, M. Markevitch, K. Matsushita, S. Allen, M. Kawaharada, B. McNamara, N. Ota, H. Akamatsu, J. de Plaa, et al., ArXiv e-prints (2014), 1412.1176.

[17] H. M. Lee, Phys. Lett. **B738**, 118 (2014), 1404.5446.

[18] K. Sigurdson, M. Doran, A. Kurylov, R. R. Caldwell, and M. Kamionkowski, Phys. Rev. **D70**, 083501 (2004), [Erratum: Phys. Rev.D73,089903(2006)], astro-ph/0406355.

[19] K. M. Nollett and G. Steigman, Phys. Rev. **D89**, 083508 (2014), 1312.5725.

[20] S. Galli, F. Iocco, G. Bertone, and A. Melchiorri, Phys. Rev. **D80**, 023505 (2009), 0905.0003.

[21] T. R. Slatyer, N. Padmanabhan, and D. P. Finkbeiner, Phys. Rev. **D80**, 043526 (2009), 0906.1197.

[22] D. P. Finkbeiner, S. Galli, T. Lin, and T. R. Slatyer, Phys. Rev. D **85**, 043522 (2012), 1109.6322.

[23] S. Galli, F. Iocco, G. Bertone, and A. Melchiorri, Phys. Rev. D **84**, 027302 (2011), 1106.1528.

[24] G. Giesen, J. Lesgourgues, B. Audren, and Y. Ali-Haimoud, JCAP **1212**, 008 (2012), 1209.0247.

[25] T. R. Slatyer, Phys. Rev. **D93**, 023527 (2016), 1506.03811.

[26] P. A. R. Ade et al. (Planck) (2015), 1502.01589.

[27] V. Barger, W.-Y. Keung, and D. Marfatia, Phys. Lett. **B696**, 74 (2011), 1007.4345.

[28] T. Banks, J.-F. Fortin, and S. Thomas (2010), 1007.5515.

[29] D. Tucker-Smith and N. Weiner, Phys. Rev. **D64**, 043502 (2001), hep-ph/0101138.

[30] R. Essig, J. Mardon, and T. Volansky, Phys. Rev. **D85**, 076007 (2012), 1108.5383.

[31] R. Essig, A. Manalaysay, J. Mardon, P. Sorensen, and T. Volansky, Phys. Rev. Lett. **109**, 021301 (2012), 1206.2644.

[32] P. W. Graham, D. E. Kaplan, S. Rajendran, and M. T. Walters, Phys. Dark Univ. **1**, 32 (2012), 1203.2531.

[33] R. Essig, M. Fernandez-Serra, J. Mardon, A. Soto, T. Volansky, and T.-T. Yu (2015), 1509.01598.

[34] P. J. Mohr, D. B. Newell, and B. N. Taylor (2015), 1507.07956.

[35] M. Steinhauser, Phys. Lett. **B429**, 158 (1998), hep-ph/9803313.

[36] N. Cabibbo and R. Gatto, Phys. Rev. **124**, 1577 (1961).

[37] H. Burkhardt and B. Pietrzyk, Phys. Lett. **B513**, 46 (2001).

[38] H. Burkhardt and B. Pietrzyk, Phys. Rev. **D84**, 037502 (2011), 1106.2991.

[39] M. Acciarri et al. (L3), Phys. Lett. **B476**, 40 (2000), hep-ex/0002035.

[40] P. Achard et al. (L3), Phys. Lett. **B623**, 26 (2005), hep-ex/0507078.

[41] V. V. Ezhela, S. B. Lugovsky, and O. V. Zenin (2003), hep-ph/0312114.

[42] M. Laine and Y. Schroder, Phys. Rev. **D73**, 085009 (2006), hep-ph/0603048.

[43] K. A. Olive et al. (Particle Data Group), Chin. Phys. **C38**, 090001 (2014).

[44] J. F. Navarro, C. S. Frenk, and S. D. M. White, Astrophys. J. **490**, 493 (1997), astro-ph/9611107.

[45] T. H. Reiprich and H. Boehringer, Astrophys. J. **567**, 716 (2002), astro-ph/0111285.

[46] D. A. Buote, F. Gastaldello, P. J. Humphrey, L. Zappacosta, J. S. Bullock, F. Brighenti, and W. G. Mathews, Astrophys. J. **664**, 123 (2007), astro-ph/0610135.

[47] E. Churazov, W. Forman, C. Jones, and H. Bohringer, Astrophys. J. **590**, 225 (2003), astro-ph/0301482.

[48] A. Burkert, IAU Symp. **171**, 175 (1996), [Astrophys. J.447,L25(1995)], astro-ph/9504041.

[49] J. M. Cordes and T. J. W. Lazio (2002), astro-ph/0207156.

[50] M. Gell-Mann and F. E. Low, Phys. Rev. **95**, 1300 (1954).